SAND2016-7202J

Journal Name

ARTICLE

Steering Microtubule Shuttle Transport with Dynamically Controlled Magnetic Fields

Received 00th January 20xx,
Accepted 00th January 20xx

DOI: 10.1039/x0xx00000x

www.rsc.org/

K.D. Mahajan,[a,†] G. Ruan[a,b,†], C.J. Dorcéna[a], G. Vieira[c], G. Nabar[a], N.F. Bouxsein[d], J.J. Chalmers[a], G.D. Bachand[d], R. Sooryakumar[c], J.O. Winter[a,e,*]

Nanoscale control of matter is critical to the design of integrated nanosystems. Here, we describe a method to dynamically control directionality of microtubule (MT) motion using programmable magnetic fields. MTs are combined with magnetic quantum dots (i.e., MagDots) that are manipulated by external magnetic fields provided by magnetic nanowires. MT shuttles thus undergo both ATP-driven and externally-directed motion with a fluorescence component that permits simultaneous visualization of shuttle motion. This technology is used to alter the trajectory of MTs in motion and to pin MT motion. Such an approach could be used to evaluate the MT-kinesin transport system and could serve as the basis for improved lab-on-a-chip technologies based on MT transport.

Introduction

Transport at the nanoscale requires overcoming challenges unique to the length scale, including Brownian motion, low Reynolds number conditions, and difficulty in directly interfacing with and manipulating structures.[1] In living organisms, such transport is achieved, at least in part, by a group of enzymes known as motor proteins that dissipate chemical energy for the active translocation of biomolecular constituents and organelles within the cytoplasm. Because of their central role in cellular transport, motor proteins have been broadly studied as a model system for achieving nanofluidic transport in synthetic and hybrid systems.[2] In particular, the intracellular transport system composed of kinesin motors and microtubule (MT) filaments has been used for the active assembly of composite nanomaterials,[3-6] as well as the development of hybrid "smart dust" sensors.[7-9]

Kinesin motor proteins consist of two heads that hydrolyze adenosine triphosphate (ATP) and propagate processively via a hand-over-hand motion along tracks formed by ~ 25 nm diameter MTs. Researchers have investigated several *ex vivo* methods to control kinesin motion, or in the inverted motility assay, MT motion on kinesin-coated surfaces. For example, the availability of fuel may be controlled using light or pH, and in turn regulate kinesin motion.[10, 11] Motion can also be inhibited by the binding of small molecules to selected regions of the kinesin molecule[12-14] or by rendering a kinesin-coated surface unable to bind MTs (i.e., through electrostatics or steric hindrance).[15, 16] All of these strategies, however, have focused on the initiation or suppression of motion, and not control of the vector of motion.

Control of *ex vivo* transport vectors has primarily relied on physical[11, 17, 18] or chemical[19] patterns to direct MT motion on kinesin-coated surfaces (i.e., the inverted motility assay). However, the majority of these approaches require lithographic patterning and permit no dynamic control over the resulting vectors, which generally limits the MT trajectories to those of the original pattern. Further, MTs can escape physical or chemical barriers, leading to stalling or undesired motion.[20] MTs have demonstrated the capability of traversing physical barriers as much as 40 times their height (e.g., up to 1 μm[11]). None of these approaches permit dynamic alteration of the trajectory of a MT in motion.

Apart from patterning approaches, control of MT vectors can be achieved by external fields, such as fluid flow,[21, 22] electrical,[23, 24] and magnetic[25-27] fields. Fluid flow has been used to align MTs in a specific orientation and to enable uni-directional transport of kinesin and associated cargoes in a pre-selected direction[21, 22]. More promising approaches toward dynamic vector regulation involve the use of external fields with the capability of investigator control. For example, Dekker et al. showed that MT trajectory could be altered by electrophoretic motion in an external electric field[24]. In the inverted motility assay, MT motion is directed by Brownian motion at the MT tip as it progresses from motor to motor. By applying an electric field to a charged tip, the trajectory of a

[a] *William G. Lowrie Department of Chemical and Biomolecular Engineering, 151 West Woodruff Avenue, The Ohio State University, Columbus, OH, 43210, USA*
[b] *Department of Biomedical Engineering, College of Engineering and Applied Sciences, Nanjing University, Nanjing, 200697, China*
[c] *Department of Physics, The Ohio State University, Columbus, OH, 43210, USA.*
[d] *Center for Integrated Nanotechnologies, Sandia National Laboratories, Albuquerque, NM, 87185, USA.*
[e] *Department of Biomedical Engineering, The Ohio State University, Columbus, OH, 43210, USA*
† Equally contributing authors
* Corresponding author email: winter.63@osu.edu
Electronic Supplementary Information (ESI) available: [details of any supplementary information available should be included here]. See DOI: 10.1039/x0xx00000x

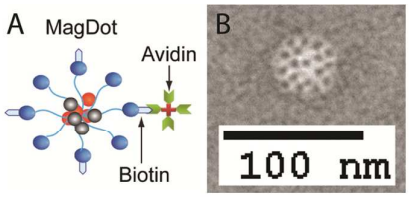

Figure 1. (A) Amphiphilic block co-polymers self-assemble in the presence of QDs and SPIONs to form micelle nanocomposites (MagDots), which are subsequently modified with biotin(B) Size and morphology of MagDots as visualized by transmission electron microscopy (TEM) with negative staining.

MT can be altered proportional to the force applied and the bending radius of the MT[28]. Inspired by this work, we investigated the potential of magnetic fields to dynamically alter MT motion.

Magnetic fields are particularly attractive for MT vector control because they can deliver programmable fields to specific micro-regions without the need for repeated lithography. Magnetic fields have been used to align MTs along magnetic field lines[29], similar to flow-based approaches,[21, 22] and to direct MT binding to a surface[27], similar to electrophoretic methods;[23] thus, combining best attributes of several alignment and steering methods. Further, proof of concept for dynamic alteration of MT trajectory has been demonstrated.[26] Hutchins et al. showed that $CoFe_2O_4$ magnetic nanoparticles attached to the leading edge of MTs may be used to alter their motion in the presence of a simple NdFeB cube magnet. In that work, altering MT trajectories was achieved by varying the separation distance between the magnet and the MTs to regulate the magnetic field strength, but with little opportunity for finely tuned, dynamic control.

Here, we examine dynamic alteration of MT motion *in situ* using programmable, micro-patterned magnetic fields. These fields can be tuned via joystick or voice commands to precisely manipulate objects ranging from ~ 10 nm to microns in size, including micro- and nano-particles and magnetically-labelled cells and molecules.[30-32] The two dimensionality of the array of microscopic patterns also enables easy platform integration with microfluidic channels and allows for single-focal plane, real time observation of individual or multiple living organisms. This manipulation set-up thus offers far more accurate selection than data averaging over a population of MT shuttles.

To render MTs gliding on a kinesin surface responsive to magnetic field gradients, MTs were combined with magnetic

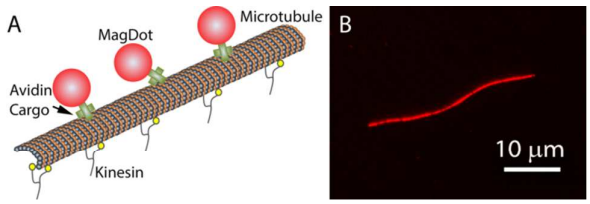

Figure 2. (A) Schematic of and (B) fluorescence image of a MT labelled with MagDots via avidin-biotin bonding.

quantum dot (i.e., MagDot) cargoes. The MagDot cargoes consist of micelles containing (1) superparamagnetic iron oxide nanoparticle (SPION) constituents that permit control of motion and (2) fluorescent quantum dot (QD) components that permit quantification through real-time optical characterization. This approach thus provides specific directional control, can potentially process multiple molecules in parallel, and integrates optical tracking with dynamic movement via the fluorescent MagDot element, permitting real time observation of MT shuttles.

Results and discussion

MagDot-Labelled Microtubules

We investigated the potential of controllable magnetic gradients to *dynamically* influence MT motion. In contrast to previous approaches,[26, 27, 33] MTs were labelled with MagDots, consisting of ~40 nm diameter block co-polymer micelles encapsulating QD and SPION nanoparticles (Figure 1A,B).[30] Thus, fluorescence signal was provided by the nanoparticle cargoes themselves, permitting MagDot organization along the MT to be characterized. MagDots were assembled on the surface of MT filaments using an avidin sandwich approach (Figure 2A,B), enabling structures with well-defined shapes to be obtained.[4] This approach enabled hierarchical assembly of nanoparticles that bridged the nano-(i.e., micellar self-assembly) to micron-length (i.e., MT filament) scales.

It has been previously reported that conjugation of nanoparticle cargoes can slow MT motion.[27, 34] Therefore, an *in situ* conjugation approach was employed in which nanoparticles are loaded onto the MTs as they are being propelled by the surface-bound kinesin motors. Because MagDots bind to exposed surfaces of kinesin-bound MTs, steric hindrance is minimized. This approach has previously been used to obviate cargo-induced slowing of MT velocity.[4, 5, 34]

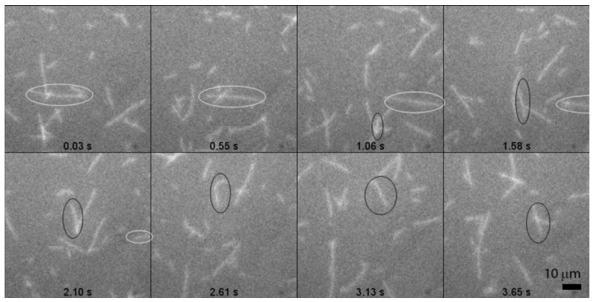

Figure 3. Transport of MTs on kinesin-coated surfaces through ATP-driven motion, demonstrating that transport of MagDots does not significantly impede MT-kinesin interactions. Two types of motion are highlighted with circles. The MT circled in white undergoes linear motion through the frames, whereas the MT circled in black exhibits circular or curved motion.

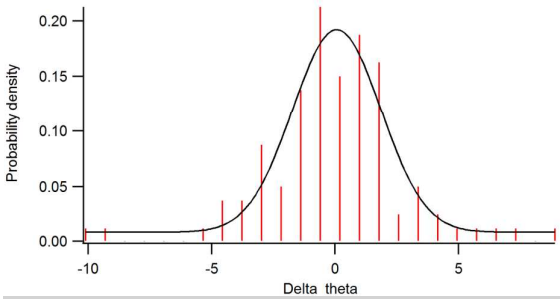

Figure 4. Histogram of the average change in theta ($\Delta\bar{\theta}$, degrees) as a function of time in the absence of a magnetic field, obtained from analysis of 100 random MTs in Movie S1. $\Delta\bar{\theta}$ is a Gaussian centred at 0.06 deg with a standard deviation of 2.52 deg, indicating the role of Brownian motion in MT steering in the absence of fields.

To confirm that transport was not affected by MagDot conjugation, cargo transport across a kinesin-coated surface was evaluated at high MT density in the gliding motility assay (Movie S1, Figure 3, Modification ratio ~ 23 MagDots/µm, calculated as described in Materials and Methods) at modification ratios of 2 to 50 MagDots/µm of MT length, representing potential surface coverages of ~ 8% to saturation (> 20, assuming 100% of MagDots attached). For example, for 100 MTs selected at random from Movie S1, the average speed was 1.4 ± 0.9 µm/s. At values above 25, MTs did not move, or if MagDots were introduced before attachment to kinesin-coated surfaces, did not attach, consistent with prior findings.[3, 34] Movement was observed for modification ratios of 5-25, whereas modification ratios lower than 2 resulted in insufficient fluorescence to view MTs. Thus, nanoparticle modification could diminish MT movement as saturation was approached, but did not appear to provide noticeable impediment to MT transport via ATP-mediated mechanisms at lower concentrations.

We also evaluated the types of motion evidenced by MTs in Movie S1, including the average change in angle as a function of time ($\Delta\bar{\theta}$) (geometry shown in Supplemental Figure 1). In the absence of magnetic fields, Brownian motion at the tip dictates MT trajectory. Thus, Gaussian behaviour would be expected. As anticipated, we observed both straight (83%) and bent (17%) MT trajectories, and $\Delta\bar{\theta}$ was a Gaussian centred at 0.06 deg with a standard deviation of 2.52 deg (Figure 4). The probability of bending is influenced by Brownian motion, but is also a function of MT length (average MT length for Movie S1 is shown in Supplementary Figure 2).

Microtubule Deflection and Capture in Dynamic Magnetic Fields

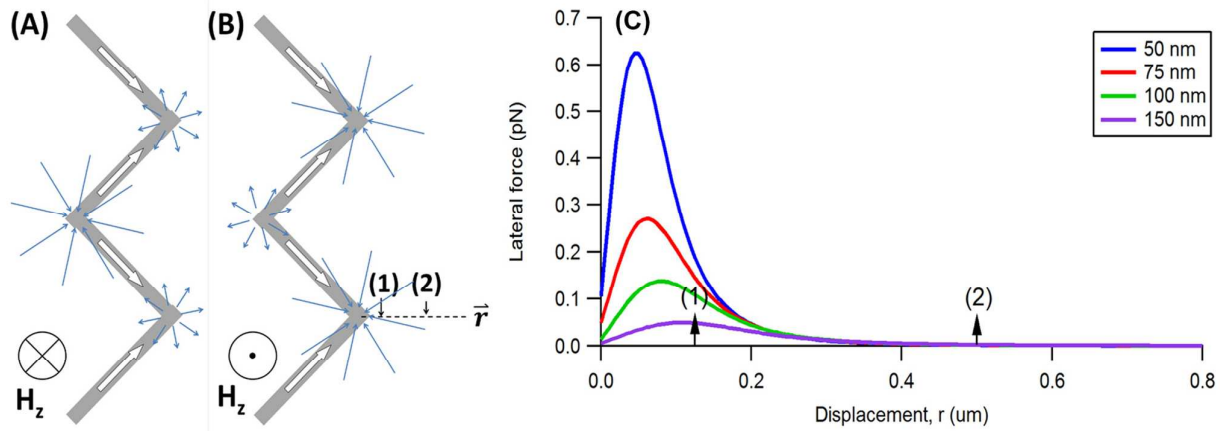

Figure 5. Illustration of trapping forces (blue arrows) for wires in different applied field configurations. (A) A zigzag wire with magnetization profile defined by the white arrows. In the presence of a downward out-of-plane applied field (Hz), vertices on the left side of the wire attract magnetic particles, while vertices on the right side are weakly repulsive. (B) Upon switching the out-of-plane field, these attributes are reversed. (C) Calculations are shown for the lateral magnetic trapping forces (F_r) on a ~50 nm-diameter MagDot to the right of a vertex, as indicated by the dotted line in (B). Forces are calculated for a MagDot with a center 50-150 nm above the plane of the wires (z direction). F_r falls quickly with increased distance from vertex ($\vec{r}$). The trapping force (1) at an $\vec{r}$ of 0.125 µm is estimated to be about 50 times larger than the trapping force (2) at an $\vec{r}$ of 0.5 µm. The lateral trapping force drops to zero at the trap centre.

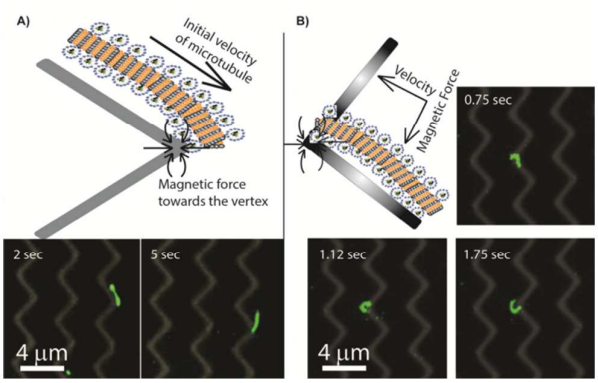

Figure 6. MT shuttle trajectories altered by applied magnetic force. A) The microassembly moves in a linear fashion, then, under the influence of the magnetic trap, is deflected and changes direction near consecutive rightward-facing vertices, continuing in a linear manner after leaving the vicinity of the vertex. In this case, the magnetic trap is not strong enough to fully capture the MT. B) When the magnetic trap is capable of fully capturing the MT, the microassembly undergoes circular motion and is contorted into a circular shape.

Control of the MT motion was achieved using tunable magnetic traps located at vertices of nanoscale zigzag cobalt-iron wires patterned onto a silicon chip. Strong magnetic field gradients near wire vertices attract constituent MagDots; and therefore, are capable of guiding MT motion toward the wire vertices. An external, out-of-plane magnetic field can strengthen the attractive magnetic force, whereas reversing the direction of this out-of-plane field weakens the attractive force or makes it weakly repulsive (Figure 5). A zig-zag micro-patterned magnetic nanowire platform was used to modify the direction of MTs undergoing ATP-driven, biological motion (Figures 6-7, Movies S2-S4) by using magnetic forces to pull MTs toward wire vertices. In addition, by modifying external magnetic fields, the force pulling the MTs could be modified, removed, or reversed, thus, permitting dynamic, investigator control of the timing and directionality of motion. In contrast, MT shuttle systems based on biological or biomimetic approaches[11] provide limited control over directionality.

We first evaluated the ability to modify trajectory as a function of MagDot modification ratio. Consistent with control experiments (Movie S1), increased MagDot modification ratio was correlated with decreases in MT speed (Table 1) (i.e., 2.8, 2.3, and 1.1 μm/s for modification ratios of 13, 20, and 23 MagDots/μm MT length, respectively). MTs did not appreciably respond to the patterned magnet vertices at modification ratios below 10 MagDots/μm.

Additionally, we observed that the ability to manipulate MT trajectory was dependent on MT length. MTs > 15-20 μm did not respond to the magnetic gradients employed in this system. Bending energy is related to MT length, L, via $E_{Bend} = k_B T L_p L/2R^2$, where k_B is Boltzmann's constant, T is temperature, L_p is the MT persistence length, R is the MT radius of curvature, so longer MTs may be more difficult to bend and steer. In particular, whereas the persistence length of MTs has reported to be 1-10 mm,[35] it has also been shown that the persistence length is inversely correlated to the contour length.[36] Thus, the inability to effectively guide long MTs with magnetic fields may be related to an increase in their persistence length and the required energy to bend and steer them. To this point, significantly straighter trajectories in the gliding motility assay have been reported when the persistence length of MTs is increased by the addition of divalent metal ions.[37] Moreover, the persistence length of

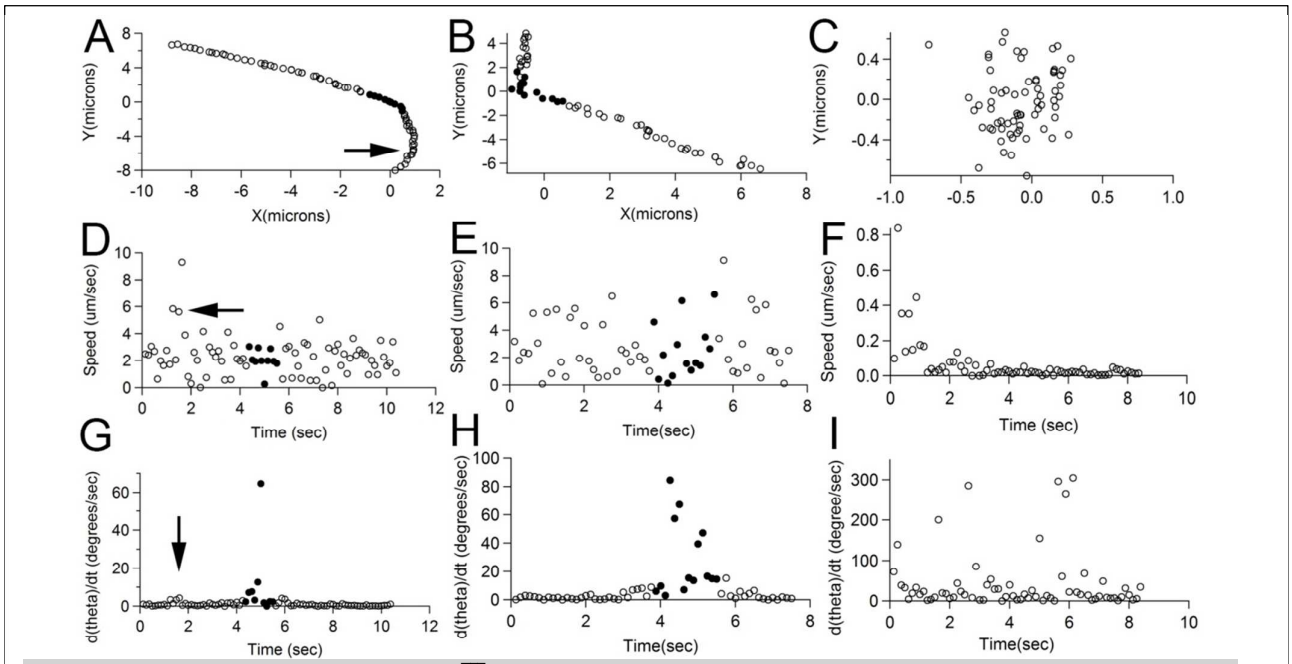

Figure 7: x-y trajectory (A-C), speed (D-F), and $\Delta\overline{\theta}/\Delta t$ (G-I) as a function of time for Movie S2 (A,D,G), Movie S3 (B,E,H), and Movie S4 (C,F,I). The point (0, 0) indicates the vertex location. For Movies S2-3 the points in black indicate interaction with a vertex (Movie S2: Vertex 2, Movie S3, Vertex). For Movie S2, arrows in A, D, and G indicate the location of vertex 1. For Movie S4, the MT interacted with a vertex during the entire viewing period.

short MTs (2-3 microns) has been shown to be significantly reduced (i.e., L_p of a few hundred microns),[36] and thus would require considerably less energy to bend and steer them with magnetic fields. The MTs observed in Movies S2-4 were short: 2.9, 2.0, and 2.7 µm, respectively.

We observed two MT behaviours resulting from modifying the trajectories of a mobile MT using engineered magnetic fields. First, upon passing nearby a vertex, a MT can deflect its motion briefly toward the vertex and continue in a straight trajectory, analogous to the unbound hyperbolic motion of a projectile attracted to a central potential (Figure 6A, Figure 7A-B, Movie S2-3, Modification ratios: 20 MagDots/µm, 13 MagDots/µm, respectively). The magnetic field varies as a function of distance from each vertex (Figure 5C); and based on analysis of the MT trajectories (Figure 7, Table 1), including speed and change in angle ($\Delta\bar{\theta}$) as a function of time, we observe magnetic steering of MTs when the distance from the vertex ($\vec{r}$) is < ~1.5 µm.

MT	NPs /µm	Frames	$\bar{v}$ (µm/s)	$\overline{\Delta\theta}$ (deg)	ϕ_{entry} (deg)	ϕ_{exit} (deg)
Movie 1, (Control)	~23	All	1.4	0.06	N/A	N/A
Movie 2, Vertex 1	20	9-14	4.5	2.30	7.7	25.6
Movie 2, Vertex 2	20	36-45	2.1	10.4	50.2	78.3
Movie 2, No Vertex	20	1-8,15-33,45-84	2.3	0.89	N/A	N/A
Movie 3, Vertex	13	32-45	2.5	28.3	0	39.3
Movie 3, No Vertex	13	1-31,45-61	2.8	2.62	N/A	N/A
Movie 4, Vertex	23	All	1.1	42.4	0	0

Table 1. Average nanoparticle loading (NPs/µm), MT speed ($\bar{v}$), change in angle with respect to the x-axis ($\Delta\bar{\theta}$), and angles of entry and exit with respect to the vertex (ϕ) with and without a magnetic field. (See Supplementary Figure 1 for geometry employed). Field is defined as active for MTs within 1.5 µm of a vertex (vertex). No field was defined as points more than 1.5 µm distant from a vertex, or points after the field was removed (no vertex).

To demonstrate investigator control of magnetic deflection, the external magnetic field was reversed, turning off the trap, at 8 and 5 s in Movie S2 and S3, respectively (frame 64 and 40, respectively). Thus, in Movie S2, the MT is initially moving in a linear trajectory, and encounters 2 vertices before the field is reversed. In both cases, θ changes rapidly in the vicinity of the vertex compared to changes at distances > 1.5 µm from vertex or without applied magnetic field (Figure 7A, D, and G; Table 1). The average speed nearly doubled near vertex 1, but was ~ 6% lower near vertex 2, possibly indicating the effect of repulsive and attractive vertices, respectively. Similarly in Movie S3, θ changes dramatically near the vertex, and speed is reduced by ~ 8% (Figure 7B, E, H). In the absence of a field or when $\vec{r}$ exceeds 1.5 µm, the MT continues in a relatively straight trajectory with little $\Delta\bar{\theta}$ because the magnetic force is sufficiently weak.

In Movies S2-3, two types of deflection responses are observed. When the MT entered the vertex parallel to the first vertex arm (ϕ_{entry} ~ 0°) then the MT exited the vertex roughly perpendicular to the vertex tip (ϕ_{exit} ~ 39°). When the MT entered the vertex roughly perpendicular to the vertex tip (ϕ_{entry} ~ 39°), then the MT was attracted to the second vertex arm, exiting parallel to it (ϕ_{exit} ~ 78°). These results clearly indicate that magnetic fields can alter MT trajectories in an investigator controlled manner.

Second, we also observed that, on rare occasions, MTs which pass close enough to a wire vertex ($\vec{r}$ < 0.5 µm) are capable of being confined to the vicinity of a wire vertex, induced to form an approximately circular shape, and made to move in an approximately circular motion near the vertex (Figure 6B, Figure 7 C, F, and I; Movie S4, Modification ratio: 23 MagDots/µm). The latter behaviour requires that MT be sufficiently close to the trap; the trap must be attractive rather than repulsive; and, the kinesin motor propulsion force must be sufficiently low that the trap force can overcome linear motion. The angular trap force is a function of $\vec{r}$ and MagDot labelling. The lateral angular trapping force rises dramatically with MT proximity to the vertex ($\vec{r}$), as our calculations indicate (Figure 5C). For example, we estimate that as the MT approaches the vertex, the attractive force on a 50 nm SPION located 150 nm above the trap surface increases by about 50 fold as it moves from an $\vec{r}$ of 0.5 to 0.125 µm (position 2 to 1, Figure 5B-C) from the vertex. Therefore, if the angular trap force is high, the ATP-mediated MT propulsion will be insufficient to escape the magnetic trap. In this case, the leading tip of the MT becomes pinned by the magnetic field, and the force of the motors pushing on the MT initiates bending of the MT into a circular shape resulting in circular motion. To the best of our knowledge, this is the first report in which a kinesin-translocated MT is deliberately pinned,[4, 24, 38] which suggests the potential use of magnetic force to temporarily "pause" transport. By reversing the magnetic field, we could potentially un-pin the MT. Such a feature suggests that engineered magnetic fields could also be exploited to create MTs with new shapes, beyond those achievable through typical manipulations.

Forces Applied to MTs by Magnetic Nanowire Traps

Although some MTs were observed to bend in the absence of magnetic fields (Movie S1), the radius of curvature observed in MTs exposed to engineered magnetic fields can be substantially smaller than that observed in the absence of magnetic forces (i.e., ~ 0.5 µm vs. 2-12 µm, Table 2). The bending energy (E_{Bend}) was calculated for each of the 3 MTs with the greatest degree of curvature in Movie S1, and these were found to be 1-2 orders of magnitude lower than the energy that could reasonably be provided by the motors (E_{Motors}), suggesting that the kinesin motors are responsible for the observed bending (Table 2, See Supplementary Material for all calculations).

To confirm the role of magnetic fields in inducing bending in Movies S2-4, E_{Bend} was calculated for each MT. In Movies S2-3, no pinning behaviour is observed and E_{Bend} is less than E_{Motors}, indicating that the magnetic force is insufficient to overcome the force provided by the kinesin motors, which could have potentially resulted in MT pinning. However, in Movie S4, E_{Bend} is 78.7 x 10^{-18} J vs. 21.2 x 10^{-18} J estimated to be provided by the motors. Thus, in this case, the magnetic force is necessary for overcoming the motor force and pinning the MT. These results clearly highlight the role of magnetic forces in generating curvature and inducing pinning behaviours. The energy contribution from the magnetic trap can also be calculated based on the magnetic field gradient and the externally applied magnetic field, if known; however, it will vary drastically based on the number of particles bound to each MT, their size, and their position relative to the vertex.

Movie-MT	L (μm)	R (μm)	E_{Bend} (J) x 10^{18}	F_{Bend} (pN)	E_{motors} (J) x 10^{18}	ΔE (J) x 10^{18}
Movie 1-1	10.6	8.68	0.87	0.08	82.9	-82.1
Movie 1-2	8.3	2.48	8.32	1.00	64.7	-56.4
Movie 1-3	11.5	11.9	0.50	0.04	89.8	-89.3
Movie 2	2.9	3.4	1.55	0.54	22.6	-21.1
Movie 3	2.0	2.0	3.04	1.56	15.3	-12.2
Movie 4	2.7	0.46	78.7	29.16	21.1	+ 57.7

Table 2: Bending energy and energy provided by motors for MTs in Movies S1-4. For Movie S1, no field is applied. Movies S2-S4 fields are applied during the first 8 s, 5 s, and the entire viewing period, respectively. The length (L) and radius of curvature (R) are reported and were used to calculate the bending energy as described in Supplemental Material. Note, that Movie S4, which displays pinning behaviour, requires substantially more force than motors are capable of providing to explain the observed behaviour, suggesting that magnetic trapping is occurring.

Conclusions

Here, we show that programmable magnetic traps can dynamically control the motion of MT shuttles. Such manipulation technology may be ideal for biological systems and biomedical applications because directional changes in motor-based transport may be induced non-invasively. This method has several advantages to other molecular transport approaches, such as force microscopy[39, 40] and molecular rockets[41, 42], because it is non-toxic and non-invasive, provides specific directional control, processes multiple molecules in parallel, and integrates tracking with the fluorescent MagDot element. This technology may be further enhanced by incorporation of microfluidics to offer more sophisticated control of flow on the magnetic arrays and permit future integration with existing lab-on-a-chip technologies. Additional biological processes beyond cytoskeletal transport, such as DNA robots, could be explored to add functionality. MT nanowire magnetic manipulation thus offers enhanced opportunities for nanofabrication, molecular separation and analysis, and single molecule research.

Experimental

Micelle Synthesis

Micelles containing nanoparticles were synthesized by the interfacial instability method as described previously.[30, 43] Briefly, 100 μl of QDs (λ_{em} = 545nm, cat No. Q 21791 MP or λ_{em} = 605 nm, cat No. Q21701 MP, Life Technologies Inc.) in decane as supplied by the manufacturer were flocculated in a mixture of 150 μl isopropanol and 300 μl methanol and re-suspended in chloroform at a concentration of 0.1 μM. Superparamagnetic Iron Oxide Nanoparticles (SPIONs) (5 nm, Cat No. SOR-05-50, Ocean Nanotech) and the amphiphilic block co-polymer carboxyl-terminated poly(styrene-b-ethylene oxide) PS(9500)-b-PEO(18000) (Cat No. P5755-SEOCOOH, Polymer Source Inc.) were separately dissolved in chloroform at concentrations of 3.45 μM and 36.4 μM, respectively. The amphiphilic polymer (10 μl, 36.4 μM), QDs (100 μl, 0.1 μM) and SPIONs (100 μl, 3.45 μM) were then mixed. Then, 210 μl organic mixture was dispersed in 800 μl of 5 mg/ml aqueous poly(vinyl alcohol) (PVA, 13,000-23,000 Dalton, 87-89% hydrolyzed, cat no. 363170, Aldrich) solution to obtain an emulsion. Chloroform was evaporated from this emulsion to obtain clear and transparent micelle dispersion.

Micelle Functionalization

Carboxylated micelles were then functionalized with biotin for MT binding via avidin-biotin bonding. Pentyl-amine biotin (Cat. No. 21345, Thermo Scientific) was conjugated to carboxylated micelles through N-(3-Dimethylaminopropyl)-N'-ethylcarbodiimide hydrochloride (EDC) chemistry.[44] Briefly, carboxylated micelle solution in water was resuspended in 2-(N-morpholino)ethanesulfonic acid (MES, Cat No. M8902, Sigma) buffer at a pH of 5.7 and was mixed with EDC (Cat No. 22980, Thermo Scientific), sulpho-N-hydroxysuccinimide (NHS) (Cat No. 24510, Thermo Scientific) and pentyl-amine biotin at the molar ratio of HOOC-PS-PEO: EDC: sulpho-NHS: Biotin 1: 1000: 2500: 100. The reaction mixture was stirred overnight at room temperature. Biotin-functionalized micelles were then dialyzed against deionized water to remove unreacted reagents.

Transmission Electron Microscopy (TEM)

Images of micelles were obtained using an FEI Tecnai G2 Bio Twin TEM. 10 μL sample droplets were pipetted onto a clean silicone pad. Samples were placed on formvar/carbon-coated nickel grids by keeping the grid over the sample droplet for 2 minutes. Phosphotungstic acid (PTA, 1%) was used for negative staining. The grid loaded with sample was placed on a 10-μl drop of PTA for 2 minutes. The excess liquid was wicked away using filter paper. The grid was then imaged and TEM images were collected.

Microtubule Polymerization

An ice-cold solution of 1 mM guanosine triphosphate (GTP, Cat No. G-8877, Sigma) and 15% glycerol dissolved in 80 mM piperazine-N,N'-bis(2-ethanesulfonic acid) (Cat No. P-6757, Sigma), 2 mM MgCl2 (Cat No. M-2670, Sigma), 1mM EGTA (ethylene glycol tetraacetic acid, Cat No. E-4378, Sigma) at pH 6.9 (BRB80) was used to suspend lyophilized tubulin proteins to 22 µM. Biotin-tubulin (Cat No. T-333P, Cytoskeleton Inc.) and unlabelled tubulin (Cat No. TL238, Cytoskeleton Inc.) were mixed at a molar ratio of 15:85 respectively and polymerized at 37ºC for 20 min. The polymerized MTs were then diluted to 0.5 µM and stabilized against depolymerization in a solution of BRB80 containing 10 µM paclitaxel (Cat No. T-7191, Sigma) and stored at room temperature.

Kinesin

Full-length D. melanogaster kinesin-1 was expressed in E. coli from the recombinant kinesin heavy chain expression vector pPK113 (http://www.ncbi.nlm.nih.gov/protein/AAD13351.1) and purified by Ni-NTA chromatography (Invitrogen). The protein concentration determined by Bradford assay was found to be 1.08 µM. Aliquots of the protein were snap frozen in liquid nitrogen and stored at -80ºC.

Motility Assays

A capillary flow chamber was constructed on a glass slide using double-sided tape and a coverslip. The average dimensions of the flow chamber were 22 mm x 3 mm x 40 µm. 5 mg/mL casein protein (Cat No. C-7078, Sigma) diluted in BRB80 were added to the flow chamber and incubated for 5 min. Kinesin was diluted to 325 nM in BRB80 with 1 mg/ml casein and 1 mM ATP (Cat No. A-2383, Sigma) and then added to the flow chamber and incubated for 5 min. Paclitaxel stabilized MTs were diluted to 0.05 µM in motility solution (BRB80 containing 5 mg/mL casein, 3 mM ATP, 0.04 mg/mL glucose oxidase (Cat No. G-2133, Sigma), 0.016 mg/mL catalase (Cat No. C-9322, Sigma), 1 mM DTT (dithiothreitol, Cat No. 161-0610, BioRad) and 40 mM D-glucose (Cat No. G-7528, Sigma)) and added to the flow chamber. Avidin target protein (Cat No. 434401, Invitrogen) (20 µl, 10^{-10} M in motility solution) was added to the flow chamber and incubated for 5 min. Biotin-functionalized micelles containing both QDs and SPIONs (i.e., biotin-MagDots) were re-suspended in motility solution, and 20 µl solution (0.1 µM) was introduced to the flow chamber and incubated for 5 minutes. 20 µl of motility solution was then flowed through the chamber to remove unconjugated micelles. After 5 min, the flow chamber was imaged on an inverted Olympus IX-71 microscope equipped with a 100X oil immersion objective and an EMCDD camera (Photometrics). All images and data were captured at room temperature.

Fabrication of Magnetic Traps

Electron beam lithography was used to pattern the magnetic structures that applied forces to MTs. Two layers of e-beam resist (methylmethacrylate and polymethyl methacrylate) were spin-coated at 4500 rpm onto silicon wafers and baked at 180 ºC for 60 s. Patterns of zigzag wires with a vertex-to-vertex distance of 4 µm and width ~400 nm were exposed using a scanning electron microscope (FEI, Hillsboro, OR, USA) and developed, followed by a deposition of 40 nm of $Fe_{0.5}Co_{0.5}$ via magnetron sputtering. An external magnetic field (~1,000 Oe) was applied to the wires and then removed to establish the magnetization profile of the wires, ensuring the creation of domain walls at each vertex. The domain wall polarity, either head-to-head or tail-to-tail, alternates at consecutive vertices.

Substrates were then coated with a 1 nm permalloy seed layer and a 5 nm gold layer by magnetron sputtering, cleaned by UV ozone for ~10 min, and incubated in a 1 mM polyethylene glycol (PEG)-SH (molecular weight 5000, Laysan Bio, Arab, AL, USA) solution in ethyl alcohol for at least 1 hr, creating a thiol-bound PEG monolayer. The surface was then rinsed in ethyl alcohol and deionized water and dried with pressurized air. The PEG monolayer aids in preventing bio-fouling and non-specific binding and increases the hydrophilicity of the surface. The substrates were then coated with ~100 nm of spin-on glass (Silicafilm, Emulsitone Co., Whippany, NJ, USA) to protect the magnetic structures and to make the surface consistent.

Magnetic Manipulation of Particles and Assemblies

A magnetic trapping and manipulation system consists of the patterned zigzag wires on a silicon substrate, two pairs of electromagnets for applying in-plane magnetic fields (H_{xy}), and a solenoid coil for an applying out-of-plane field (H_z). The out-of-plane field acts to strengthen, weaken, or reverse the magnetic traps (Figure 5). The system was mounted on the stage of a reflected fluorescence microscope (Olympus BX 41). A 5-µl sample drop was placed on the substrate, which was covered with a coverslip and immersion oil. An out-of-¬plane field (H_z) of ~100 Oe was applied upward, which allows magnetic particles to be trapped at specific locations. At selected time points, the direction of H_z was switched by reversing the current in the solenoid coil, moving magnetic structures between wire vertices.

Fluorescence Imaging

Fluorescent imaging was performed using an Olympus IX71 fluorescent microscope with a 100x oil immersion objective, a 100 W mercury lamp, λ_{ex} = 488 nm, long-pass emission filter, and an EMCDD camera (Photometrics).

Image Processing and Analysis

Image processing and analysis was conducted using Image J image analysis software by combining brightfield background images showing the wire arrays with fluorescence images showing the MTs. For each movie, the x, y positions of MTs were evaluated as a function of time and used to calculate the average MT speed and $\Delta\bar{\theta}$ as a function of time. For Movie S1, 10 randomly selected MTs in each 50 sequential frames were evaluated for a total of 100 MTs, whereas the displayed MTs were evaluated in Movies S2-4.

Calculation of MagDot Modification Ratio

The number of MagDots per unit MT length was calculated by determining the integrated fluorescence intensity from the frame of highest intensity (to minimize effects of quantum dot blinking) and dividing by the average fluorescence intensity of a single MagDot, as described previously.[45]

Acknowledgements

The authors gratefully acknowledge the support of the National Science Foundation, grant numbers: CMMI-0900377, DMR-1206745, EEC-0914790, DMR-0820414, the U.S. Army Research Office under Contract W911NF-14-1-0289, the Ohio State University Nanoscale Science and Engineering Center for Affordable Nanoengineering of Polymeric Biomedical Devices EEC-0914790, Materials Science and Engineering Research Center for Emergent Materials DMR-0820414, and the Institute for Materials Research, a "Thousand Young Global Talents" award from the Chinese Central Government, Priority Academic Program Development Fund of Jiangsu Higher Education Institutions (PAPD), Nanjing University and the "Tian-Di" Foundation, College of Engineering and Sciences, Nanjing University, China. This work was performed, in part, at the Center for Integrated Nanotechnologies, an Office of Science User Facility operated for the U.S. Department of Energy (DOE) Office of Science, project number C2011B21. Sandia National Laboratories is a multi-program laboratory managed and operated by Sandia Corporation, a wholly owned subsidiary of Lockheed Martin Corporation, for the U.S. Department of Energy's National Nuclear Security Administration under contract DE-AC04-94AL85000.

Notes and references

1. E. R. Kay, D. A. Leigh and F. Zerbetto, *Angewandte Chemie-International Edition*, 2007, **46**, 72-191.
2. G. D. Bachand, N. F. Bouxsein, V. VanDelinder and M. Bachand, *WIREs Nanomed. Nanobiotechnol.*, 2014, **6**, 163-177.
3. G. D. Bachand, S. B. Rivera, A. K. Boal, J. Gaudioso, J. Liu and B. C. Bunker, *Nano Lett.*, 2004, **4**, 817-821.
4. H. Liu, E. D. Spoerke, M. Bachand, S. J. Koch, B. C. Bunker and G. D. Bachand, *Adv. Mater.*, 2008, **20**, 4476-4481.
5. H. Liu and G. D. Bachand, *Soft Matter*, 2011, **7**, 3087-3091.
6. O. Idan, A. Lam, J. Kamcev, J. Gonzales, A. Agarwal and H. Hess, *Nano Lett.*, 2012, **12**, 240-245.
7. G. D. Bachand, H. Hess, B. Ratna, P. Satir and V. Vogel, *Lab Chip*, 2009, **9**, 1661-1666.
8. T. Fischer, A. Agarwal and H. Hess, *Nat. Nanotechnol.*, 2009, **4**, 162-166.
9. P. Katira and H. Hess, *Nano Lett.*, 2010, **10**, 567-572.
10. H. Higuchi, E. Muto, Y. Inoue and T. Yanagida, *Proc. Natl. Acad. Sci. U. S. A.*, 1997, **94**, 4395-4400.
11. H. Hess, J. Clemmens, D. Qin, J. Howard and V. Vogel, *Nano Lett.*, 2001, **1**, 235-239.
12. Y. Miyamoto, E. Muto, T. Mashimo, A. H. Iwane, I. Yoshiya and T. Yanagida, *Biophys. J.*, 2000, **78**, 940-949.
13. A. Nomura, T. Q. P. Uyeda, N. Yumoto and Y. Tatsu, *Chem. Commun.*, 2006, DOI: 10.1039/b606538d, 3588-3590.
14. K. R. S. Kumar, T. Kamei, T. Fukaminato and N. Tamaoki, *ACS Nano*, 2014, **8**, 4157-4165.
15. B. D. Martin, L. M. Velea, C. M. Soto, C. M. Whitaker, B. P. Gaber and B. Ratna, *Nanotechnology*, 2007, **18**.
16. L. Ionov, M. Stamm and S. Diez, *Nano Lett.*, 2006, **6**, 1982-1987.
17. H. Suzuki, K. Oiwa, A. Yamada, H. Sakakibara, H. Nakayama and S. Mashiko, *Japanese Journal of Applied Physics*, **34**, 3937.
18. Y. Hiratsuka, T. Tada, K. Oiwa, T. Kanayama and T. Q. P. Uyeda, *Biophys. J.*, 2001, **81**, 1555-1561.
19. B. Rupp and F. Nedelec, *Lab Chip*, 2012, **12**, 4903-4910.
20. J. Clemmens, H. Hess, J. Howard and V. Vogel, *Langmuir*, 2002, **19**, 1738-1744.
21. K. J. Bohm, R. Stracke, P. Muhlig and E. Unger, *Nanotechnology*, 2001, **12**, 238-244.
22. R. Yokokawa, S. Takeuchi, T. Kon, M. Nishiura, K. Sutoh and H. Fujita, *Nano Lett.*, 2004, **4**, 2265-2270.
23. I. Dujovne, M. van den Heuvel, Y. Shen, M. de Graaff and C. Dekker, *Nano Lett.*, 2008, **8**, 4217-4220.
24. M. G. L. van den Heuvel, M. P. de Graaff and C. Dekker, *Science*, 2006, **312**, 910-914.
25. M. Platt, G. Muthukrishnan, W. O. Hancock and M. E. Williams, *J. Am. Chem. Soc.*, 2005, **127**, 15686-15687.
26. B. M. Hutchins, M. Platt, W. O. Hancock and M. E. Williams, *Small*, 2007, **3**, 126-131.
27. B. M. Hutchins, M. Platt, W. O. Hancock and M. E. Williams, *Micro Nano Lett.*, 2006, **1**, 47-52.
28. N. Isozaki, S. Ando, T. Nakahara, H. Shintaku, H. Kotera, E. Meyhöfer and R. Yokokawa, *Scientific reports*, 2015, **5**, 7669.
29. M. Platt, G. Muthukrishnan, W. O. Hancock and M. E. Williams, *J. Am. Chem. Soc.*, 2005, **127**, 15686-15687.
30. G. Ruan, G. Vieira, T. Henighan, A. R. Chen, D. Thakur, R. Sooryakumar and J. O. Winter, *Nano Lett.*, 2010, **10**, 2220-2224.
31. G. Vieira, T. Henighan, A. Chen, A. J. Hauser, F. Y. Yang, J. J. Chalmers and R. Sooryakumar, *Phys. Rev. Lett.*, 2009, **103**, 128101.
32. K. D. Mahajan, G. B. Vieira, G. Ruan, B. L. Miller, M. B. Lustberg, J. J. Chalmers, R. Sooryakumar and J. O. Winter, *Chem. Eng. Prog.*, 2012, **108**, 41-46.
33. B. M. Hutchins, W. O. Hancock and M. E. Williams, *Phys. Chem. Chem. Phys.*, 2006, **8**, 3507-3509.
34. M. Bachand, A. M. Trent, B. C. Bunker and G. D. Bachand, *J. Nanosci. Nanotechnol.*, 2005, **5**, 718-722.
35. T. Hawkins, M. Mirigian, M. Selcuk Yasar and J. L. Ross, *J. Biomech.*, 2010, **43**, 23-30.
36. F. Pampaloni, G. Lattanzi, A. Jonáš, T. Surrey, E. Frey and E.-L. Florin, *Proceedings of the National Academy of Sciences*, 2006, **103**, 10248-10253.
37. N. F. Bouxsein and G. D. Bachand, *Biomacromolecules*, 2014, **15**, 3696-3705.
38. H. Hess, J. Clemmens, C. Brunner, R. Doot, S. Luna, K. H. Ernst and V. Vogel, *Nano Lett.*, 2005, **5**, 629-633.
39. D. M. Eigler and E. K. Schweizer, *Nature*, 1990, **344**, 524-526.
40. K. C. Neuman and A. Nagy, *Nat. Methods*, 2008, **5**, 491-505.
41. R. F. Ismagilov, A. Schwartz, N. Bowden and G. M. Whitesides, *Angewandte Chemie International Edition*, 2002, **41**, 652-654.

42. T. R. Kline, W. F. Paxton, T. E. Mallouk and A. Sen, *Angew. Chem. Int. Ed. Engl.*, 2005, **44**, 744-746.
43. G. Ruan and J. O. Winter, *Nano Lett.*, 2011, **11**, 941-945.
44. G. T. Hermanson, *Bioconjugate Techniques*, Academic Press, San Diego, 1996.
45. A. D. Duong, G. Ruan, K. Mahajan, J. O. Winter and B. E. Wyslouzil, *Langmuir*, 2014, **30**, 3939-3948.